Energy 293 (2024) 130718

Contents lists available at ScienceDirect

Energy

journal homepage: www.elsevier.com/locate/energy

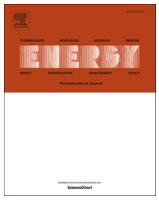

Concentrated solar heat for the decarbonization of industrial chemical processes: a case study on crude oil distillation

Claudia Prestigiacomo [a], Alberto Giaconia [b], Federica Proietto [a], Giampaolo Caputo [b], Irena Balog [b], Egnazio Ollà [c], Chiara Freni Terranova [c], Onofrio Scialdone [a], Alessandro Galia [a,*]

[a] Dipartimento di Ingegneria, Sezione Chimica Ambientale Biomedica Idraulica e dei Materiali, Università degli Studi di Palermo, Viale delle Scienze, 90128, Palermo, Italy
[b] ENEA-Casaccia Research Center, via Anguillarese 301, 00123, Rome, Italy
[c] Raffineria di Milazzo SCPA (RAM) - Contrada Mangiavacca, Milazzo, 98057, ME, Italy

ARTICLE INFO

Keywords:
Chemical industry
Topping
Decarbonization
Concentrating solar plant
Solar heat

ABSTRACT

A novel strategy for the decarbonization of crude oil distillation was proposed considering two distillation columns located in Sicily that were simulated by adapting the equipment datasheet of the refinery Raffineria di Milazzo (RAM). The proposed approach consists of the integration of the topping section with a concentrating solar power (CSP) plant to decrease the carbon dioxide emissions and the consumed fossil fuels in the furnaces of the distillation columns. Three hypothetical scenarios of applicative interest were considered. In that most economically sustainable, the use of solar heat allowed a decrease of CO_2 emissions of 54.2 kt/year corresponding to a reduction of about 11% of the greenhouse gas emissions joined with the saving of 19.9 kt/year of methane with a rate of return of investment (ROROI) of 16.2%. As a comparison, if the land surface occupied by the CSP plant is used for photovoltaic production of green hydrogen considering an energy consumption of the electrolyzer of 4.70 kWh/Nm^3, just 24.6 and 9.0 kt/year of CO_2 and methane respectively can be saved and the ROROI decreases to 8.5%.

This study indicates that solar heat can be effectively and economically integrated in crude oil distillation to achieve a significant decarbonization of refineries.

1. Introduction

The industrial sector accounted for 38% of the total energy consumption in 2022 [1]. Chemical and petrochemical industries are among the largest energy consumers with an average annual growth of energy demand in the period 2000–2016 of 2% associated with a 2.5% yearly rate of increase in CO_2 emissions [2].

Petrochemical products have essential roles in many applications related to health care, transportation, food, electronics, and many clean energy technologies and are considered by IEA the largest driver of global oil demand [3].

Even if the use of fossil fuel will be gradually ruled out, refineries energy-intensive processes will be on for several decades, as crude oil-based fuels will continue to be necessary for transportation [4]. Furthermore, in the roadmap to zero net CO_2 emissions, refineries will still be important in the energy economy after being converted to bio-refineries to produce liquid biofuels for jet fuel [5,6]. In this framework, one of refineries' major problem is the reduction of CO_2 emissions. Recently, Wang et al. [7] reported that the global potential of using solar heat as renewable source of energy in the oil operations varies from 17 to 44 GW in the upstream sector and from 21 to 95 GW in downstream operations.

Instead, Altayib and Dincer [8] studied the possibility of decreasing the consumption of fossil fuels to pre-heat crude-oil using a solar-based integrated cogeneration system. This route includes crude-oil heating and power generation via a steam Rankine cycle with an overall energetic and exergetic efficiencies of 60.94% and 19.34%, respectively [8].

Another investigated alternative is to employ parabolic trough collectors (PTC) integrated with a thermal energy storage system to generate solar steam to keep the temperature of heavy crude oil products before despatching from storage tanks [9]. PTC without storage system were also considered to pre-heat the process fluid in a gas refinery saving about 24 % of the fuel consumption of the furnace [10] or to investigate transient modeling and optimization of lubricant oil refinery site utility systems with regard to solar energy [11].

* Corresponding author.
E-mail address: alessandro.galia@unipa.it (A. Galia).

https://doi.org/10.1016/j.energy.2024.130718
Received 15 October 2023; Received in revised form 13 February 2024; Accepted 14 February 2024
Available online 17 February 2024

Abbreviations

Alb	ground albedo
ANI	aperture normal irradiance (W/m^2)
CAPEX	capital expenditures (€)
COM	cost of manufacturing (€)
CSP	concentrated solar plant
d_k^{DDB}:	depreciation at year k
DBB	double declining balance depreciation method
DiffH	diffuse horizontal irradiance (W/m^2)
DNI	direct normal irradiance (W/m^2)
$\varepsilon_{CO_2}^{Fuel_j}$:	emission factor (kg GHG/TJ)
$E_{nd}L_{oss}$	end loss effects
$E_{(column_i)}^{Fuel_j}$:	fuel consumption (TJ)
$E_{100\%}^{Furnace_i}$:	energy consumed by the furnace i when it operates at 100% of the nominal power (TJ)
E^{solar} :	energy provided by the concentrated solar plant (TJ)
GHG	Green House Gases
GHI	global horizontal irradiance (W/m^2)
GI_{PV}	global irradiance on the PV module (W/m^2)
HTF	heat transfer fluid
j	type of fuel
K_{mod}	incidence angle modifier
L_f	focal length (m)
L_P	length of parabolic trough (m)
LHV	low heating value (kJ/kg)
$M_{CO_2}^{Fuel_j}$:	mass of carbon dioxide for each kind of consumed j type of fuel (kg)
ME	module efficiency
N	total number of years
i	the number of loops
OPEX	operating expenditures (€)
$P_{100\%}^{Furnace}$:	nominal power of the furnace (W)
$P^{solar\ plant}$:	nominal operating power provided by the concentrated solar plant (W)
PV	photovoltaic
RAM	Raffineria di Milazzo
ROROI	rate of return of the investment (%)
$R_{ow}S_{hadow}$	shadowing effect
ϑ:	incidence angle of solar radiation
ϑ_z:	solar zenith angle
t_{month}:	operating time of the distillation units without coupling with CSP per month (h)
$t_{month}^{solar\ plant}$:	operating time of the solar plant per month (h)
T_{in}^{cold}:	inlet temperature of the cold stream (crude) in the molten salts heat exchangers (°C)
T_{out}^{cold}:	outlet temperature of the cold stream (crude) in the molten salts heat exchangers (°C)
T_{in}^{hot}:	inlet temperature of the hot stream (molten salt mixture) in the molten salts heat exchangers (°C)
T_{out}^{hot}:	outlet temperature of the hot stream (molten salt mixture) in the molten salts heat exchangers (°C)
TMY	typical meteorological year
W	aperture width (m)
q	flow rate of HTF in each loop (kg/s)
Q	total HTF flow rate collected from the hot TES that is split in Q1 and Q2 (kg/s)
Q1	flow rate sent to molten salt heat exchanger network of unit 1 (kg/s)
Q2	flow rate sent to molten salt heat exchanger network of unit 2 (kg/s)

The distillation of crude oil is one of the most energy-consuming processes of a refinery as about 30–40% of its total energy demand is used in this unit operation [12]. The main factors that determine the energy consumption are the size of the distillation columns and the quality of the crude oil. Up to 20% reduction of the energy consumption can be achieved by the improvement of heat integration among the different process streams [13].

In the aforementioned context, the availability of economically sustainable strategies to decarbonize refineries is highly necessary and the use of solar heat could be an interesting option to decrease their carbon footprint.

In spite of this awareness, the practical implementation of the integration is complex and not obvious because requires the development of a strategy to match economically the intermittent nature of sun radiation with its continuous running. In the literature a few studies and reviews have been published on the integration of solar heat in industrial processes at low-medium temperature with special focus on the food [14–16] and pulp and paper industry [17].

As far as we know, no study to investigate the feasibility of the integration of a concentrating solar power (CSP) plant with crude oil distillation has been published in the open literature.

The scientific contribution of our study is the definition of a process lay-out and the formulation of a generally applicable strategy to integrate high temperature solar heat collected by a CSP plant, based on current state of the art technology, in the topping section of a crude oil refinery.

The study was completed with a techno-economic analysis carried out using as a reference the design data of *Raffineria di Milazzo* (RAM) located in Milazzo in Southern Italy. Then we estimated the impact of the integration on the CO_2 emission and fuel consumption and assessed its economic sustainability. The estimations were repeated under the hypothesis that the same refinery would be located in the United Arab Emirates to study the impact of local solar irradiation on the economic sustainability.

2. Methodology

2.1. Design of the concentrating solar plant

The CSP is based on linear PTC consisting of 100 m long Solar Collector Assemblies (SCA) with 5.8 m effective mirrors' width, according to a design demonstrated by ENEA in previous projects [18]. Accordingly, a mixture of molten nitrates ($NaNO_3/KNO_3$, 60/40 w/w), namely the "solar salt", has been considered as heat transfer fluid (HTF) and heat storage medium up to 550 °C [19].

Fig. 1 shows the general scheme of the CSP considered in this work. It consists of several loops (80 or 100 loops, as explained in the following sections) composed of six SCA, each 100 meters long. Therefore, in total, the HTF has 600 m of linear active pathway in each loop of the receiver tubes to collect the concentrated solar radiation. Thermal insulation of the piping is made of ceramic blanket (inner layer, 50 mm) and mineral wool (outer layer, from 50 to 120 mm). The molten salt is pumped from the cold tank (around 290 °C) to the solar field to be heated up to 550 °C and then, collected in the hot storage tank. Thermal insulation of the tanks is made of ceramic fiber (two inner layer, 50 mm each) and mineral wool (five consecutive layers, 100 mm each).

The first input parameter to design the CSP is the direct normal irradiance (*DNI*). The typical meteorological year (TMY) for solar radiation has been calculated using a methodology described by Dribssa et al. [20]. The TMY consists of twelve typical meteorological months

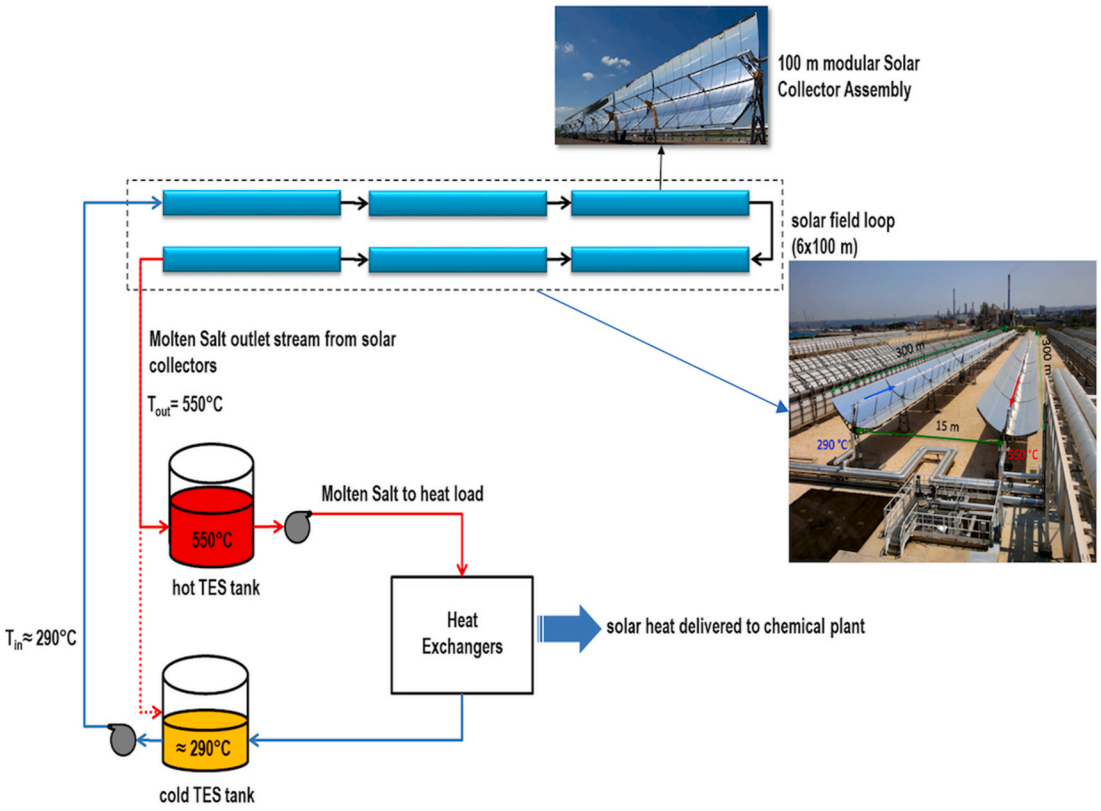

Fig. 1. Scheme of one solar collector loop and block diagram of the molten salt loop to the heat load.

(TMM). Each TMM is selected from various calendar months in a multi-year weather database by the nonparametric method known as Finkelstein-Schafer statistics comparing the yearly cumulative distribution function with the long-term cumulative distribution function in the month concerned. In this study, the Global Horizontal Irradiation database obtained from satellite image processing (METEOSAT) from 2006 to 2022 was used.

The work herein was developed using two different sequences (2006-2022): the TMY *DNI* sequence in Sicily (Milazzo, 38.2 N, 15.26 E) where the annual cumulative DNI is 1940.5 kWh/m^2/year and that of a specific site in the United Arab Emirates (Solar Park 24.77 N, 55.44 E) where the annual cumulative *DNI* is 2,387.7 kWh/m^2/year.

As described in the following paragraphs, besides the higher overall *DNI* level yearly, the Middle East site is characterized by a more uniform solar irradiation during the year that is expected to improve the fraction of solar energy available to drive the distillation.

To study the possibility of replacing part of the energy used to drive the atmospheric distillation of crude oil with solar heat from a CSP plant, a collaboration with the RAM refinery located in Sicily between Milazzo and San Filippo del Mela (Messina) was established.

The RAM provided the design data of the crude oil distillation equipment implemented in the refinery thus allowing to set values of applicative interest for the required thermal powers. These data are the second input parameters necessary to determine the size of the CSP plant.

To design it and its coupling with the chemical process, the fraction of incident solar radiation actually collected by the surface of the receiver tubes, namely the Aperture Normal Irradiance (*ANI*), was determined for each *DNI* sequence. The *ANI* is lower than the *DNI* because it includes only the mirror-normal solar radiation component, proportional to the cosine of the angle between the direction of the sun's rays and the normal direction to the collector. The *ANI* also considers the shading effect between solar collectors that depends on the distance between their rows.

The *ANI* distribution was calculated from *DNI* using the Eq. (1):

$$ANI = DNI \times K_{mod} \times R_{ow}S_{hadow} \times E_{nd}L_{oss} \quad (1)$$

where K_{mod} is the incidence angle modifier that is given by an empirical equation obtained from the fitting of experimental data for a given type of collector, $R_{ow}S_{hadow}$ provides the shadowing effect, and $E_{nd}L_{oss}$ the end loss effects due to incomplete reflection of the incoming sun rays on the solar receiver in the ends of linear solar collector rows.

In the case of collectors considered in this study, typically adopted by ENEA, the fitting equation to determine K_{mod} is reported in Eq. (2):

$$K_{mod} = \cos\vartheta + 9.511E-4 \times \vartheta - 3.218E-5 \times \vartheta^2 \quad (2)$$

where ϑ is the incidence angle of solar radiation, i.e. the angle formed by the direction of the beam radiation on a surface and the normal direction to that surface. The incidence angle will vary over the day, as well as throughout the year, and will heavily influence the scavenging performance of the collectors.

$R_{ow}S_{hadow}$ and $E_{nd}L_{oss}$ in Eq. (1) can be determined by Eq. (3) and (4):

$$R_{ow}S_{hadow} = \left(L_{spacing} \,/\, W\right) \times \left(\cos\vartheta_z \,/\, \cos\vartheta\right) \quad (3)$$

where $L_{spacing}$ is the center distance of two parabolic trough concentrators, W is the aperture width (5.8 m) and ϑ_z is the solar zenith angle.

$$E_{nd}L_{oss} = 1 - \left(L_f \times \tan\vartheta \,/\, L_p\right) \quad (4)$$

where L_f is the focal length and L_P is the length of the parabolic trough (having values of 1.81 and 100 m respectively in the solar field under consideration).

In Fig. 2a the as-determined typical *ANI* sequence in Milazzo is reported. Calculation were conducted with the PTC technology considered by ENEA in previous studies [18,21].

In Milazzo an average value of the *ANI* specific collected solar power of 173.6 W/m^2 was found with a maximum radiation value of 966 W/m^2

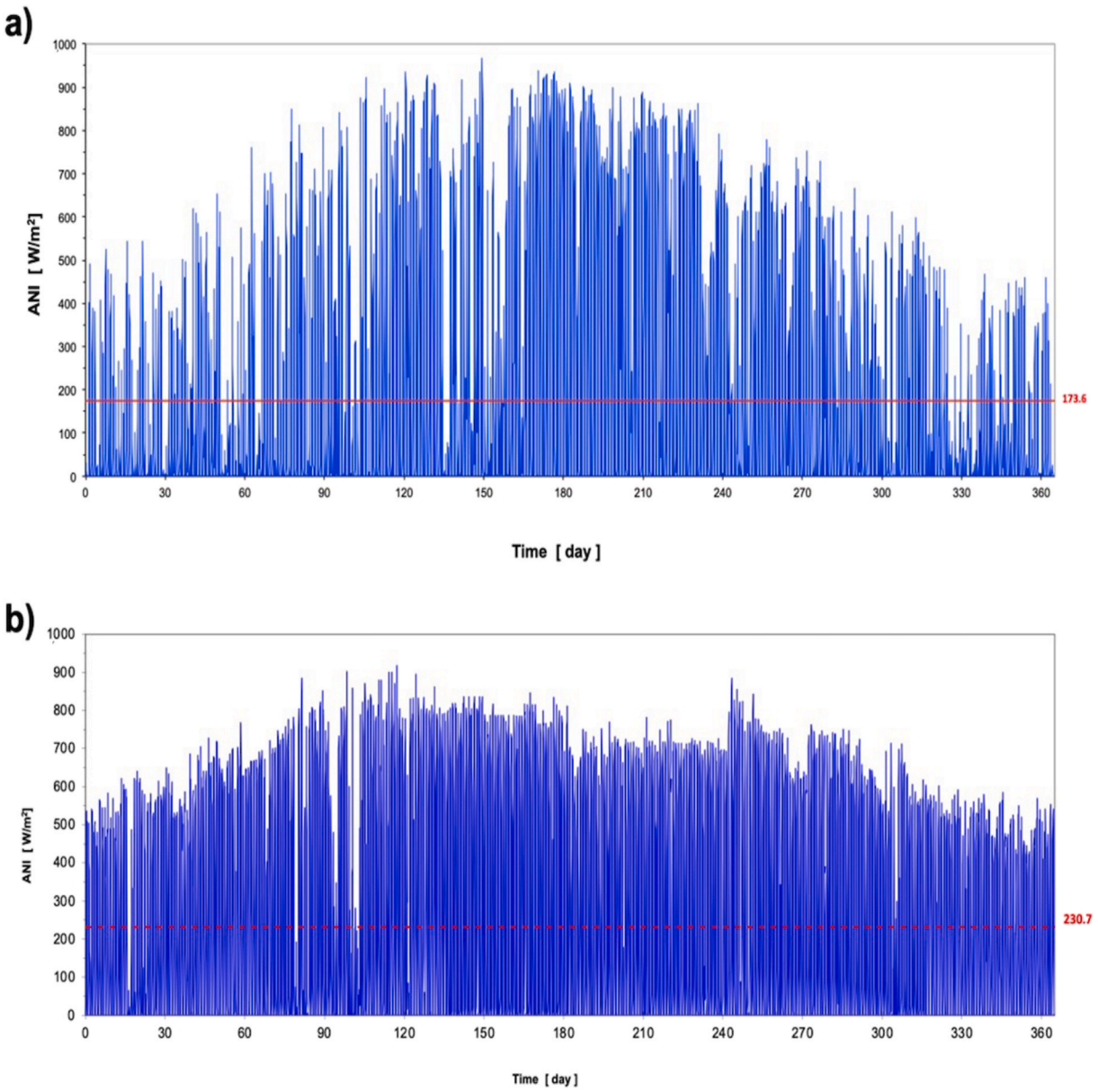

Fig. 2. a) *ANI* sequence over the year in Milazzo; b) *ANI* sequence over the year in the selected site in the United Arab Emirates.

obtained in May and an annual integral value of 1,521.6 kWh/(m^2 y). In Fig. 2b is plotted *ANI* for the case of an oil refinery site located in the United Arab Emirates. The annual integral value is 2,021.5 kWh/(m^2 y), the maximum radiation value is 918 W/m^2, and the average value is 230.7 W/m^2.

The monthly distributions of the daily mean value of *ANI* in the two sites are plotted in Fig. 3.

It is noteworthy that the two sites do not significantly differ in the maximum daily direct radiation intensity, but rather in the distribution of the solar irradiation over the year, which is more evenly distributed in the Middle East site.

Fig. 4 shows the annual hourly distribution of the *ANI*, i.e. the number of hours in a year in which direct solar irradiation can be captured; this parameter is approximately 3,800 h in Milazzo and 4,100 h in the United Arab Emirates.

For a given value of the *ANI*, the flow rate of the molten salt is adjusted to obtain the target temperature of 550 °C in each loop of the solar field: the lower the *ANI*, the lower the molten salt flow rate to reach the target temperature. A minimum flow rate of 1.5 kg/s was fixed for the molten salt in each loop: therefore, when the ANI falls below a threshold value (e.g. after sunset or during cloudy periods) the molten salt flow is circulated in each parallel loop at its minimum rate of 1.5 kg/s and, if the outlet temperature of 550 °C could not be reached, the outlet molten salt (at T < 550 °C) is recirculated to the cold tank.

The efficiency of the solar field is defined as the thermal energy effectively transferred to the HTF divided by the normal irradiance on collectors, i.e. the *ANI* (W/m^2) multiplied by the effective reflecting area of collectors; typical factors affecting the efficiency of the solar field have been considered, including solar tracking errors, geometric factors, the reflectance of clean mirrors, receiver tubes absorbance, dust effects on mirrors reflectance and receiver tubes absorbance, etc.

The operation of a modular design of this kind of solar field has been recently demonstrated by ENEA [18].

The larger the number of 600 m length rows connected in parallel, the larger the daily captured solar heat and the number of hours during which the chemical process can be sustained with it, provided that the TES is large enough to store all captured enthalpy at 550 °C. This matching extends the chemical plant operation with solar heat for a

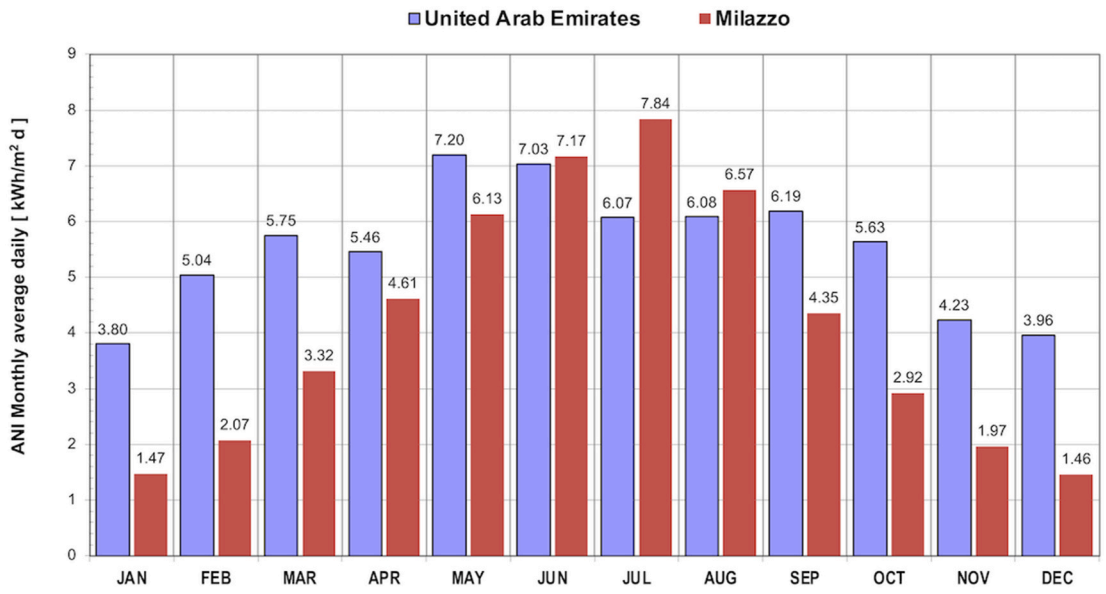

Fig. 3. Comparison of monthly distribution of the daily mean value between the two selected sites in Milazzo (red) and United Arab Emirates (light purple).

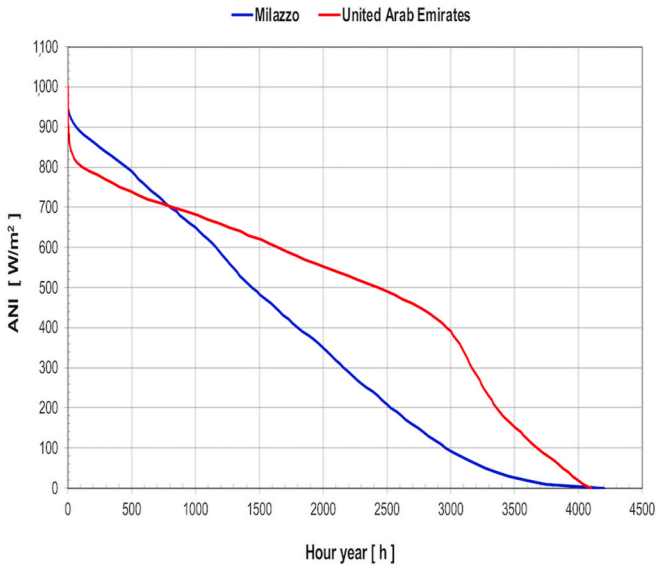

Fig. 4. Difference Distribution of the *ANI* over the year between the two selected sites in Milazzo (Blue continuous line) and United Arab Emirates (Red line).

number of hours when the *DNI* drops.

Considering the aforementioned solar irradiance data and the required thermal load of the topping section, the area of the solar field (i.e. the number of collectors) was determined and the effect of its coupling with the atmospheric distillation in term of the reduction of tons of emitted CO_2 and consumed fuel was studied.

2.2. Design of photovoltaic field

To evaluate the decarbonizing efficacy of the integrated process considered in this study we estimated the amount of green hydrogen that can be produced using renewable electricity generated by a PV field covering the same land surface necessary for the solar plant.

The input data for the sizing of the PV field are the *DNI*, the Diffuse Horizontal Irradiance (*DiffH*), the Global Horizontal Irradiance (*GHI*) and the ground albedo that corresponds to the coefficient of reflection of the ground (in this case equal to 0.2) (*Alb*).

The TMY for solar radiation (*GHI*, *DNI* and *DiffH*) was calculated from EUMETSAT satellite imagery (2006-2022) based on a methodology described by Dribssa et al. [20]. As mentioned in the previous section of this work, two TMY sequences (2006-2022) were considered: the TMY (*GHI*, *DNI* and *DiffH*) in Sicily (Milazzo, 38.2 N, 15.26 E) and the TMY (*GHI*, *DNI* and *DiffH*) in a specific site in the United Arab Emirates (Solar Park 24.77 N, 55.44 E).

The Global Irradiance on the PV module (GI_{PV}) was calculated using Eq. (5):

$$GI_{PV} = DNI_{PV} + Diff_{PV} + Alb_{PV} \quad (5)$$

where DNI_{PV} is the bean irradiance, $Diff_{PV}$ is the diffuse irradiance on the PV module and Alb_{PV} is the albedo arriving on the PV module.

DNI_{PV} was obtained as a function of *DNI* and of the incidence angle of solar radiation ϑ by Eq. (6):

$$DNI_{PV} = DNI \times \cos\vartheta \quad (6)$$

To estimate $Diff_{PV}$ the isotropic model, which assumes a uniform distribution of the diffuse irradiance from the sky vault, was adopted:

$$Diff_{PV} = DiffH \times ((1 + \cos\vartheta_{tilt}) / 2) \quad (7)$$

where ϑ_{tilt} is the tilt angle of the PV module.

Alb_{PV} was calculated considering the fill factor in front of the module:

$$Alb_{PV} = GHI \times Alb \times ((1 - \cos\vartheta_{tilt}) / 2) \quad (8)$$

The PV power output P_{PV} was estimated from the GI_{PV} assuming a constant module efficiency ME_{PV}:

$$P_{PV} = ME_{PV} \times GI_{PV} \times A \quad (9)$$

where A is the area of the PV module.

Flash test of manufacturer had given a measured module efficiency of 0.2. To estimate the ME_{PV} we considered an inverter efficiency equal to 0.95 and all other losses equal to 0.05, so that the cumulative module efficiency of the PV panel ME_{PV} is equal to 0.18.

2.3. Hybridization of the distillation unit with the CSP plant

The distillation units of RAM can treat two different crude oil qualities through two parallel process chains each equipped with an

atmospheric distillation column and with a furnace.

In both process lines the crude oil is pre-heated by heat integration with side streams extracted from the topping columns.

More in detail, one of the distillation units, labeled "Topping 3", was designed to treat 920–960 t/h of crude oil and it is equipped with a horizontal cabin that can supply up to 139.5 MW heating the crude oil from 230-240 °C to 360–370 °C, using fuel gas. A second distillation unit labeled "Topping 4" was designed to treat 760–840 t/h of crude oil and it is equipped with a horizontal cabin with maximum power similar to that of the previous furnace (139.6 MW) but burning a mixture of fuel oil and refinery fuel gas to heat the crude oil from 240-250 to about 370 °C.

Starting from these design data we developed a simulated case study based on two hypothetical distillation columns that will be named "Unit 1" and "Unit 2" adapting information taken from RAM technical reports that are summarized in Table 1.

In the simulated study, the furnace of unit 1 (furnace 1) was considered fueled with methane while that of unit 2 (furnace 2) was considered fueled with a mixture constituted by 80% fuel oil and 20% methane. These assumptions do not represent the real RAM operating conditions but are still meaningful from the applicative viewpoint.

The coupling of the topping units with the CSP plant was made by the intermediacy of the HTF. In particular, the hot molten salt mixture of $NaNO_3/KNO_3$ (60/40 w/w) heated at 550 °C in the solar collectors was used to transfer the solar heat to the crude oil in a train of heat exchangers inserted in the process lines between the heat exchangers networks using side streams to pre-heat the crude and the furnaces (Fig. 5).

The number, size, configuration and oil temperatures in these additional heat exchanger networks are reported in Table 2 and were estimated by the software Aspen Plus® using the chemico-physical properties listed in Table S1 and the routine described in Aspen plus, "Getting Started Modeling Petroleum Processes" Report [22]. Molten salt mixture was modeled as "energy stream" of the heat exchanger units in Aspen Plus ® and its properties were defined by referring to an earlier study by ENEA [23].

A CSP plant using molten salt as HTF is equipped with a backup boiler to heat the mixture at the design temperature of 550 °C even when the solar irradiation is not enough. This option ensures a continuous energy supply to the service duty.

The hybridization strategy proposed in our study was planned to work without a backup boiler with the topping section that can operate just in two alternative ways (managed with an on/off logic):

- 100% operation of the CSP: a fraction of the thermal energy is powered by the CSP and the furnace works at reduced power to complete the heating and vaporization of the crude at inlet conditions of the topping column (Table 2).
- 0% operation of the solar system: the crude oil distillation unit is powered only by the furnace that works at its nominal power.

Then when the solar irradiation was not enough to heat the molten salts flowing in the receivers till the target temperature of 550 °C, the HTF is recirculated from the hot storage tank to the coldest and the enthalpy to drive distillation is entirely supplied by the furnaces.

RAM confirmed the possibility of tuning the power of typical topping furnaces with power flexibility ranging from 50% to 100% of the design value. This knowledge is essential to make possible that the same ovens already operating in the refinery can be adapted to the hybridized plant.

Following this strategy, different configurations of the CSP plant were considered (Table 3) by changing the integrated solar power from 50 to 70 MW and the extension of the solar field (80 and 100 strings of 6 solar collectors each) by setting a maximum capacity of the hot storage tanks to 800,000 KWh.

2.1.1. Techno-economic assessment of the hybridized topping section

Mass and energy balances were performed to determine the global energy requirements of the process.

To assess the economic sustainability of the proposed strategy, a market survey was carried out to estimate the costs of methane (the most used fuel), fuel oil, and the cost that the refinery must pay annually for the quantities of CO_2 emitted into the atmosphere.

It has been found that at the end of 2021, the average cost of methane was about 1,169 €/ton, the cost of fuel oil 521 €/ton while the cost of the certificate for the emission of one ton of CO_2 was around 96 €/ton.

The tons of CO_2 emitted by the unit without coupling with the solar system (traditional oven at full power) and those emitted considering the integrated solar system (traditional oven and molten salt exchangers) were estimated.

The calculation of the tons of CO_2 emitted by the furnaces was made following the simplest approach reported in IPCC guidelines of 2006 [24] using the concepts of fuel consumption ($E^{Fuel_j}_{(column_i)}$) and emission factor $\varepsilon^{Fuel_j}_{CO_2}$ as reported in Eq. (10):

$$M^{Fuel_j}_{CO_2} = E^{Fuelj} \times \varepsilon^{Fuel_j}_{CO_2} \tag{10}$$

where $M^{Fuel_j}_{CO_2}$ represents the mass (kg) of CO_2 emitted for each kind of consumed j type of fuel (kg of greenhouse gases GHG), $E^{Fuelj}_{(i)}$ is the j fuel consumption expressed in TJ i.e. the energy developed by the burned fuel and $\varepsilon^{Fuel_j}_{CO_2}$ is the emission factor of the j fuel (kg GHG/TJ).

The emission factors were 56,100 kg/TJ for natural gas and 73,300 kg/TJ for fuel oil [24].

The cumulative fuel consumption E^{Fuel} to supply non-solar enthalpy to both furnaces per each month of the year was determined as follows:

$$E^{Fuel} = E^{Furnace}_{100\%} - E^{Solar} \tag{11}$$

where all quantities are expressed in TJ, $E^{Furnace}_{100\%}$ is the energy consumed by the furnaces when they run at 100% of the operating power and E^{Solar} is the energy provided by the solar plant to the topping columns according to the considered scenarios. $E^{Furnace}_{100\%}$ and E^{Solar} were calculated by Eq. (12) and (13) respectively:

$$E^{Furnace}_{100\%} = P^{Furnace}_{100\%} \times t_{month} \tag{12}$$

$$E^{Solar} = P^{Solar} \times t^{solar\ plant}_{month} \tag{13}$$

$P^{Furnace}_{100\%}$ is the cumulative operating power of the furnaces, P^{Solar} represents the nominal operating power provided by the solar plant to the

Table 1
List of operating parameters considered in the case study.

Information about the configuration of the atmospheric crude oil distillation plant section (topping).		
Number of distillation columns (labeled throughout the text with the term "unit")	2	
Number of furnaces used in each unit	1	
	Unit 1	**Unit 2**
Design capacity of the units (t/h)	960.5	843.5
Temperature of the feed entering the furnace (°C)	240	246
Temperature of the feed entering the column (°C)	370	368

Specifications of crude oil heating furnaces connected to units.		
	Unit 1	Unit 2
Operating thermal power (MW)	131	109
Fuel	methane	80% fuel oil 20% methane
LHV (kJ/kg)	47,409	9,698 (fuel oil)/47,409
Total exchanging surface	(1,858 m^2 radiant zone) (445 m^2 convective zone)	(2,128 m^2 radiant zone) (445 m^2 convective zone)
Furnace	Horizontal cabin	Horizontal cabin

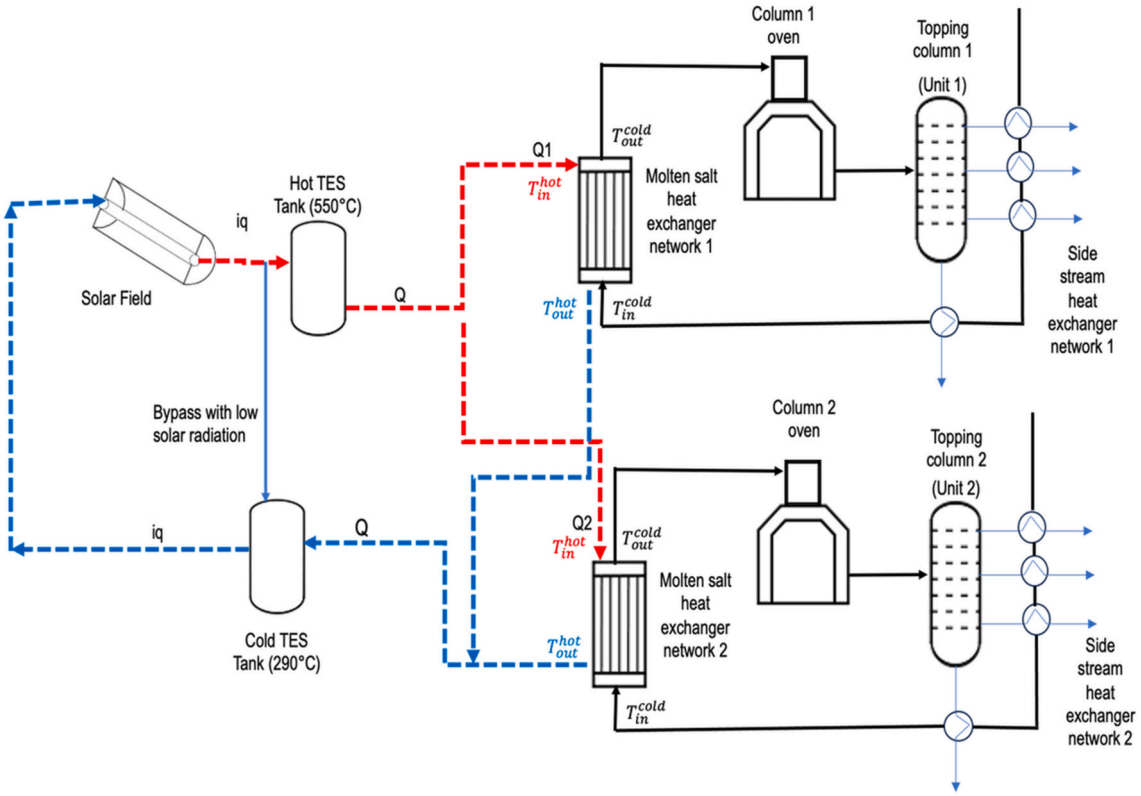

Fig. 5. Scheme of the on/off hybridization strategy: i is the number of loops, q is the flow rate of HTF in each loop (minimum value 1.5 kg/s), Q is the total HTF flow rate collected from the hot TES that is split in Q1 sent to molten salt heat exchanger network of unit 1 and Q2 sent to molten salt heat exchanger network of unit 2, T_{in}^{cold}: inlet temperature of the cold stream (crude oil) in the molten salts heat exchangers, T_{out}^{cold}: outlet temperature of the cold stream (crude oil) in the molten salts heat exchangers, T_{in}^{hot}: inlet temperature of the hot stream (molten salt mixture) in the molten salts heat exchangers, T_{out}^{hot}: outlet temperature of the hot stream (molten salt mixture) in the molten salts heat exchangers.

Table 2
Characteristics of heat exchangers networks (HEN) powering unit 1 and 2 (showed in Fig. 5) cold stream: crude oil; hot stream: molten salts.

	Scenario 1		Scenario 2	Scenario 3
	HEN 1[a]	HEN 2[b]	HEN 1[a]	HEN 2[b]
Total exchange area (m^2)	368	366	902	589
Number of shells (series sequence)	2	2	2	2
T_{in}^{cold} (°C)	240	246	240	246
T_{out}^{cold} (°C)	268	275	308	294
T_{in}^{hot} (°C)	550			
T_{out}^{hot} (°C)	300			

[a] HEN connected to Unit 1.
[b] HEN connected to Unit 2.

distillation columns in each scenario, t_{month} is the operating time of the distillation units without coupling with CSP in each month and $t_{month}^{solar\ plant}$ is the operating time of the solar heat supply per each month. The powers were expressed in TW and times in seconds.

The assessment of the coupling of the industrial process with CSP was made following the Discounted Cash Flow method. The capital investment cost (CAPital EXpenditure - CAPEX) of the solar system was estimated by ENEA staff based on internal skills and tools.

The investment costs related to heat exchangers and furnaces were calculated using the cost indices. The OPEX, also called the production cost or cost of manufacturing (COM), of the CSP was estimated at 0.03 USD/kWh (i.e. 0.027 €/kWh) as reported in the IRENA report on the analysis of renewable energy costs [25].

The purchased cost of molten salt heat exchangers was estimated by Aspen Process Economic Analyzer.

The rate of return of investment (ROROI) which represents the undiscounted rate at which the money is obtained from the investment of fixed capital considered, was estimated as per Eq. (14), following an analysis of the cash flow considering a plant life of 10 years, with production starting from the 2nd year being the first dedicated to the construction of the solar plant.

$$ROROI = Averaged\ annual\ net\ profit / CAPEX \quad (14)$$

where CAPEX is the capital expenditures of the plant. The calculations

Table 3
Synoptic table of the coupling strategies of a CSP with the simulated crude oil distillation unit.

Scenario	Thermal power of CSP (MW)	Number of solar loops	Maximum temperature of HTF (°C)	Distillation unit	Total thermal power of furnace (MW)	Reduced thermal power of the furnaces (%)
1	70	100	550	Unit 1; Unit 2	131.2 MW (Unit 1); 109.1 MW (Unit 2)	Unit 1: reduction of 27% Unit 2: reduction of 32 %
2	70	100	550	Unit 1	131.2 MW	reduction of 43 %[a]
3	50	80	550	Unit 2	109.1 MW	reduction of 46 %[a]

[a] the other distillation unit is conventionally operated with its own furnace.

were made assuming an investment interest rate of 10% and a revenue tax rate of 40%. Depreciation costs were considered using the Double Declining Balance Depreciation Method, DDB over 10 years, calculated with equation (15):

$$d_k^{DDB} = \frac{2}{n} \times \left[CAPEX - \sum_{j=0}^{j=k-1} d_j \right] \quad (15)$$

Where d_k^{DDB} is the depreciation at year k, calculated with the DDB depreciation method, and n represent the total years.

3. Results and discussion

The large amount of energy required to drive the distillation unit hinders the possibility that the furnaces are entirely substituted by CSP because in this case a very large solar field would be needed that makes the strategy anti-economic and very case sensitive as it is difficult to have a large extension of free space near existing plants. As a rule of thumb, the largest size of CSP plants to supply solar heat to industrial processes is limited to 100 loops, corresponding to about 330,000 m^2 of surface of collectors, which was then the value considered in this study. Considering a typical land coverage factor of 0.5 for parabolic trough collectors (i.e., the ratio between the active surface of collectors and the land area), this upper limit corresponds to a solar field of 66 hectares of dedicated land size and larger areas do not seem realistic for practical reasons.

Additionally, with a solar field of 330,000 m^2 it is possible to supply steadily the process with 50–70 MW of solar heat, including the loading of thermal energy storage for 24 hours of operation during sunny periods minimizing the periods of defocusing of solar collectors and then with the highest rate of utilization of concentrated solar radiation for the target power of this study.

With these premises, hybridization seemed the most promising route to achieve decarbonization without a significant economic penalty. Three different scenarios were considered (Table 3). The first two are based on the same CSP plant and they differ only in the distribution of the solar heat between the two distillation units. In the first case (scenario 1), the solar heat was equally divided to the furnaces of units 1 and 2, while in the second case (scenario 2) it was sent entirely to unit 1. The third case (scenario 3) was built up considering that all the solar heat is sent to unit 2. In the last case, since the total thermal power of the furnace was 109 MW and considering that the maximum allowable thermal power reduction of a furnace is around 50 %, it was necessary to decrease the number of solar strings and then the collected thermal power of the CSP.

3.2. Solar field

A first evaluation was performed by analyzing the behavior of the solar plant for each case study described in Table 3. The *ANI* sequences calculated from available *DNI* were used to size the solar plant and obtain the total amount of solar heat, stored as enthalpy of the molten salt mixture, that can be powered to the selected distillation unit.

The outcomes obtained in each scenario were reported in Table S2 according to *DNI* sequence of Milazzo and of United Arab Emirates in terms of the number of hours of full operation of the furnace, the number of hours of dumping (i.e. defocusing of concentrators) and the number of hours of solar integration all calculated per each month of the year

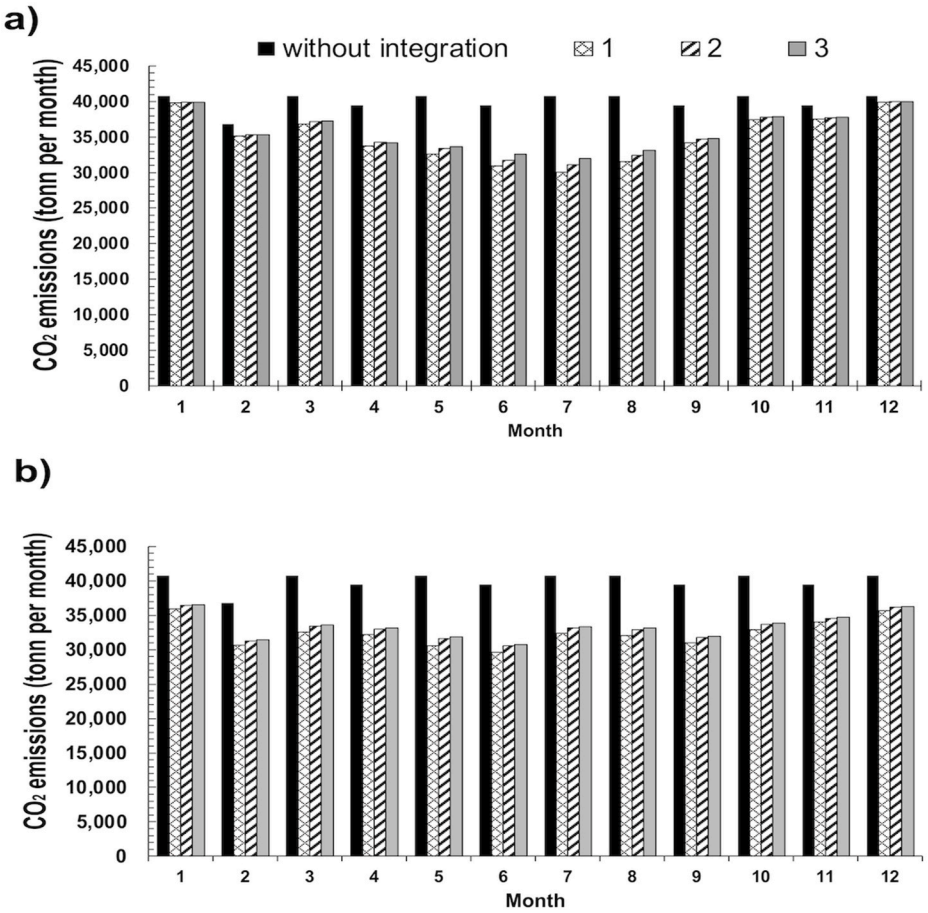

Fig. 6. Monthly CO_2 emissions for traditional distillation unit (without integration) and for the hybridized plant according to scenarios 1, 2 and 3 listed in Table 3 with *DNI* sequences a) from Milazzo (Sicily) b) from United Arab Emirates.

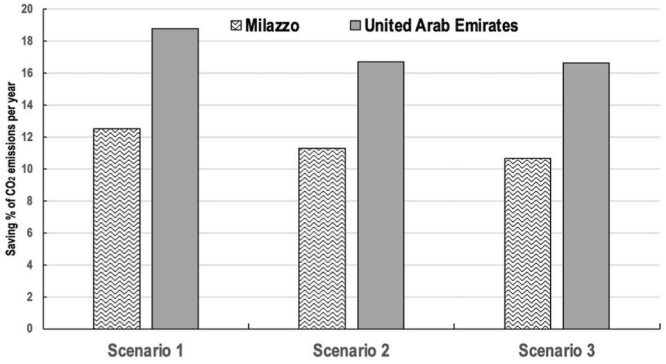

Fig. 7. Percentage of tons of CO_2 saved by hybridization with the CSP in scenarios 1, 2 and 3 of Table 4 with *DNI* sequence from Milazzo (Sicily) and United Arab Emirates.

(month 1 is January and 12 is December). As the nominal power for the coupling of the topping unit in scenarios 1 and 2 is the same the solar plants have the same size. Thanks to more uniform solar irradiation over the year the CSP located in the United Arab Emirates reached a higher average percentage of operation of the solar plants (last column on the right in Table S2).

3.3. Assessment of the decarbonization strategies

The decarbonization strategy proposed in the work herein is based on the substitution of part of the thermal power of the traditional furnaces with solar heat thus decreasing the amounts of burned fuel and of produced CO_2.

The on/off strategy described in the section of methods allowed us to estimate the non-solar power needed for the integration in the three analyzed cases. The collected outcomes regarding the distribution of the hours of operation of the solar integration were used to estimate the CO_2 emissions per month and distillation column by Eq. (10).

The calculated furnace, solar and fuel energy are listed in Table S3 as a function of the month of the year. It is possible to observe that in all the investigated cases, the integration strategy has a significant effect on the reduction of CO_2 emissions (Fig. 6). The Scenario 1 is the most advantageous because the solar heat is divided into both distillation columns thus decreasing the thermal duty of furnace of unit 2 that, for the development of the study, was supposed to use 80% of fuel oil, as reported in the design data sheet, having an emission factor 230% higher than that of methane.

The best results in terms of reduction of CO_2 emissions were observed in scenario 1 (Fig. 7) under the hypothesis that a refinery with the same design data is located in United Arab Emirates. In this case, 89,000 tons of CO_2 can be saved in one year thanks to the hybridization that are about 19% of those emitted in the absence of solar integration. Also in the case of the refinery plant located in Sicily a significant CO_2 emission reduction, ranging from 11 to 13%, can be estimated.

3.4. Economic assessment

A preliminary economic analysis based on the Discounted Cash flow method was conducted for the case studies coupled with the DNI of Milazzo considering the tons of CO_2 not emitted and fuel not consumed as the only source of profit. In Table 4 and Fig. 8, the CAPEX evaluation and the Discounted Cash flow diagrams obtained by the economic analysis for the coupling of the solar plant with the crude oil distillation unit are reported respectively. The outcomes indicate that, for the *DNI* of Milazzo, scenario 2 is the most promising since it would allow a ROROI of 16.2%, higher than 12.6 and 10.6% of scenarios 1 and 3 respectively. This advantage can be associated with the fact that the thermal load in case 2 is entirely used in the topping line whose furnace runs with methane only. The price of methane considered in this study, in fact, is about double that of fuel oil.

3.5. Comparison of the decarbonization effect on refinery of solar heat and green hydrogen

A large emission source in refineries is the steam methane reformer (SMR) which must supply hydrogen to perform hydrotreating and upgrading of heavy distillation cuts [26]. To assess the decarbonizing efficacy of the process proposed in this study we estimated the amount of green hydrogen that can be produced using renewable electricity generated by a PV field covering the same land surface necessary for the solar plant with 100 loops.

We estimated a cumulative annual productivity of 136,606,000 kWh of electric energy that was distributed during the year as depicted in Fig. 9.

To estimate the amount of hydrogen produced with the PV field we considered that the specific energy consumption owing to ohmic losses and overvoltages in real PEM electrolyzers ranges from 4.00 to 5.50 kWh/Nm^3 referred to hydrogen with a minimum limiting thermodynamic value of 3.17 kWh/Nm^3 [27].

To conduct the evaluation we used the thermodynamic value for the best possible outcome and an average value of 4.70 kWh/Nm^3 as representative of the performance of a real electrochemical reactor.

Table 4
CAPEX and OPEX evaluation for the coupling of the solar plant with crude oil distillation unit.

	Scenario 1	Scenario 2	Scenario 3
Nr. of solar collectors	100		80
Nominal Power of solar plant (MW)	70		50
Area of the solar plant (m^2)	327,398.40		261,918.72
Cost due to the solar collectors and piping	44.2 M€		35.4 M€
Cost of the pump	3.3 M€		2.8 M€
Cost of the valves	1.9 M€		1.5 M€
Cost of the salts	9.9 M€		7.1 M€
Cost of the storage tank	1.2 M€		1.1 M€
Other expenditures (auxiliary electrical heating system, insulation, measurement & control system, etc.)	0.3 M€		0.2 M€
Cost of the civil works due to the solar plant	6.3 M€		5.0 M€
Purchased cost of molten salt heat exchanger networks	2.4 M€ (Unit 1) 2.6 M€ (Unit 2)	6.3 M€	4.3 M€
CAPEX	72.1 M€	73.4 M€	57.4 M€
OPEX	6.2 M€	6.2 M€	4.8 M€
Savings of CO_2 (tonn/anno)	60,141.2	54,228.8	51,197.2
Saved fuel (tonn/anno)	11,979 t/year of methane; 8,200 t/year of fuel oil	19,859 of methane	3,178 t/year of methane; 12,711 t/year of fuel oil

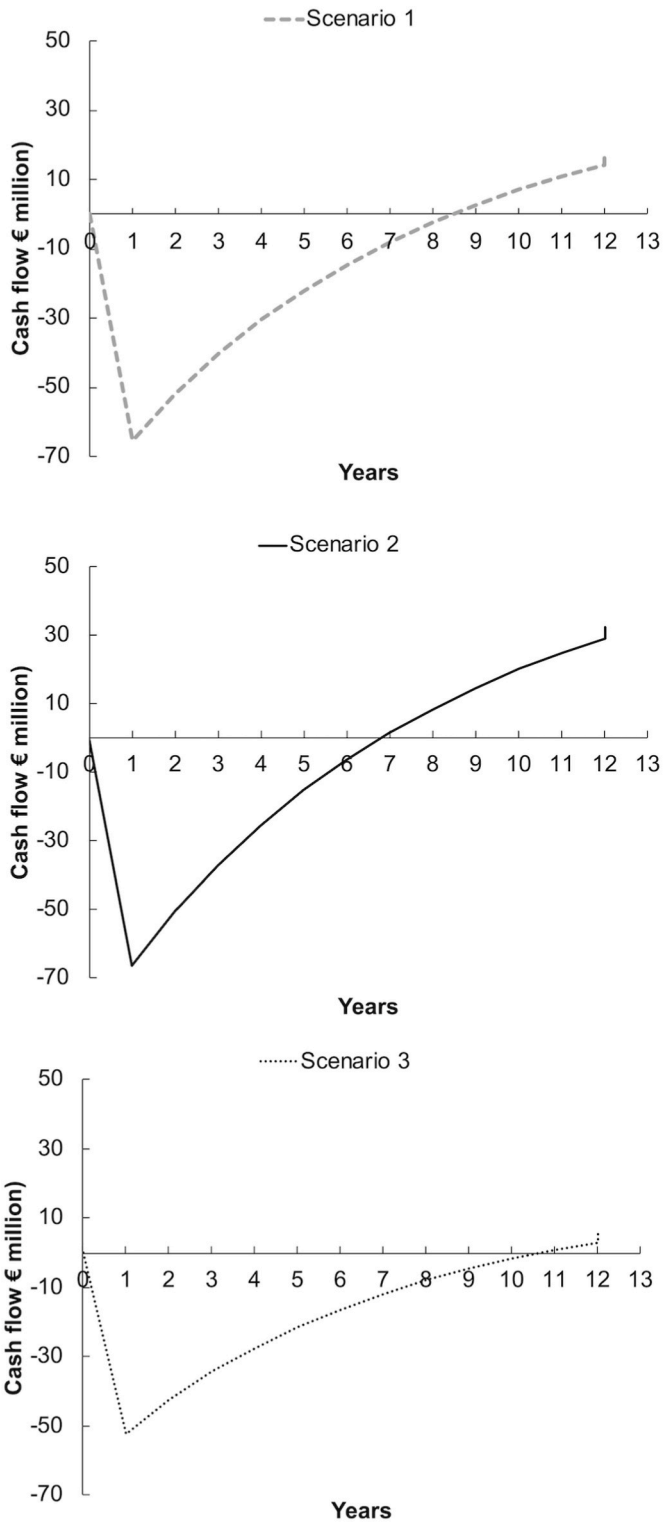

Fig. 8. Discounted cash flow diagrams obtained by the economic analysis of scenarios in Table 3.

As traditional technology, we considered the allothermal steam reforming of methane followed by water gas shift using the hydrocarbon also to feed burners of the furnace supplying enthalpy for the endothermic route.

In this case for each kt of generated H_2 an average production of CO_2 of 9–10 kt was estimated arising from methane utilization as feedstock (Eq. 16 and 17) and as a fuel (Eq. (18)) [26,28]:

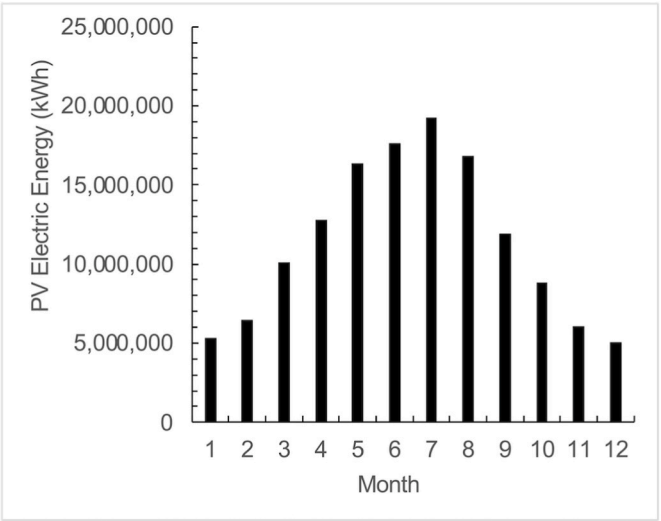

Fig. 9. Annual distribution of productivity of electric energy from PV.

$$CH_4 + H_2O \rightarrow CO + 3H_2 \qquad \Delta H\ (298\ K) = 206\ kJ/mol \tag{16}$$

$$CO + H_2O \rightarrow CO_2 + H_2 \qquad \Delta H\ (298\ K) = -41\ kJ/mol \tag{17}$$

$$CH_4 + 2\,O_2 \rightarrow CO_2 + 2\,H_2O \qquad \Delta H\ (298\ K) = -880\ kJ/mol \tag{18}$$

Using as a reference the average value of 9.5 kt CO_2/kt H_2 corresponding to a consumption of 3.5 kt CH_4/kt H_2 in reactions (16) and (18) we estimated for real electrolyzers a reduction in CO_2 emissions of 24.6 kt together with a saving of methane of 9.0 kt (Table 5).

These values are lower than 50% of that achievable if solar heat captured with the same land surface is used to drive energetically the topping columns.

From the economic point of view, one can estimate the ROROI of the PV and electrolyzer scenario considering that the stack of electrochemical reactors is sized to run continuously with an annual energy consumption corresponding to the cumulative amount of electric energy generated by the PV field i.e. with a power of the cell stack of 72 MW.

The CAPEX of the electrolyzer ranges from 500 to 1,000 USD per kW [29] and an average value of 750 USD/kW was assumed in this study while the OPEX was taken as 3% of CAPEX [29]. Values of CAPEX for PV changes from 460 €/kW [30] to 1,000 €/kW [31] and the average value of 730 €/kWh was then considered with an OPEX that can be estimated at 2% of CAPEX in both reports. [30,31]

With these values, the Discounted Cash flow method already adopted to estimate ROROI of hybridization of topping with solar heat was extended to the production of green hydrogen obtaining values reported in Fig. 10.

It can be observed that, even in the case of the thermodynamic limiting condition, the ROROI of the green hydrogen scenario was slightly lower than the best one based on the use of solar heat for decarbonization.

Then we found that direct use of solar heat to drive the topping section of a refinery is a strategy that can offer a higher reduction of the CO_2 emissions and fuel savings with a faster recovery of the investment with respect to the hypothesis of using the same land space for green hydrogen production (see Fig. 11)

4. Conclusions

In this study, we proposed and assessed a process lay-out and a plant conduction strategy to integrate significant amount of solar heat in the energy intensive topping section of a refinery.

Using an intermittent hybridization strategy the most economically

Table 5
Values of reduction in CO_2 emissions together with a saving of methane in the case of a real electrolyzer.

	Energy consumption H_2 (kWh/Nm^3)	H_2 produced (kmol)	H_2 produced (kt)	Saved CO_2 emissions (kt)	Reduced CH_4 consumption (kt)
	3.17	1,922,645.4	3.85	36.5	13.3
	4.70	1,296,763.0	2.59	24.6	9.0
Scenario 2 (Solar heat)				54.2	19.9

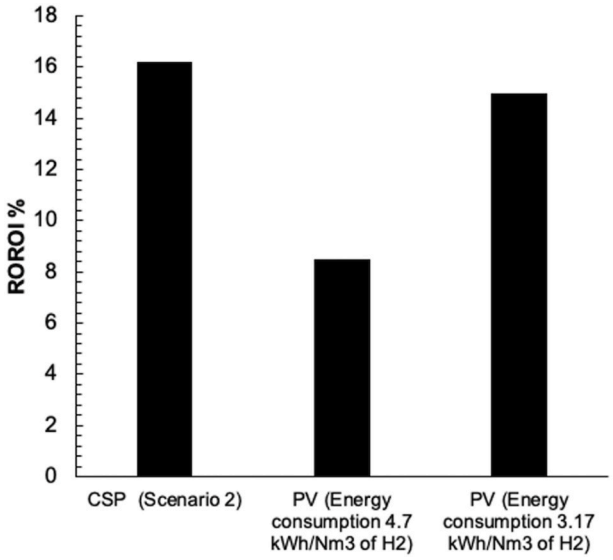

Fig. 10. Values of ROROI for the production of green hydrogen.

sustainable scenario was obtained when the whole amount of solar enthalpy is used to decrease the thermal load of a methane-fueled furnace heating the crude before its inlet in the distillation column. In this case, a pay-back time of 6 years was estimated with an annual reduction of 54.2 kt of CO_2 emitted corresponding to 11 % of the total greenhouse gas emissions of the considered methane-fueled unit, and 19.9 kt of consumed methane.

If the same refinery configuration was located in a more insulated region like United Arab Emirates using the same design data a significant increment of the decarbonization efficacy could be obtained with the same investment and operative costs as the fractional reduction of CO_2 emissions of the distillation units increases from the 11% of Sicily to 17%.

To challenge the value of the direct utilization of solar heat as a decarbonizing agent we considered that the same land surface used for the CSP plant is covered with PV panels and the generated electric energy is used to synthesize green hydrogen in substitution of that coming from methane steam reforming.

In the case of PV-based strategy, the reduction of CO_2 emissions and CH_4 consumptions were estimated about one-half of those achieved by direct injection of solar heat in the topping section with a ROROI that ranged from 15.0 to 8.5, depending on the efficiency of the electrolyzer unit, always lower than that obtained with the integrated CSP.

These results demonstrate that it is possible to find a process lay-out that make possible the direct utilization of solar heat in refineries and that can be an economic sustainable option to achieve decarbonization, particularly for plants that are located in regions with high solar irradiation.

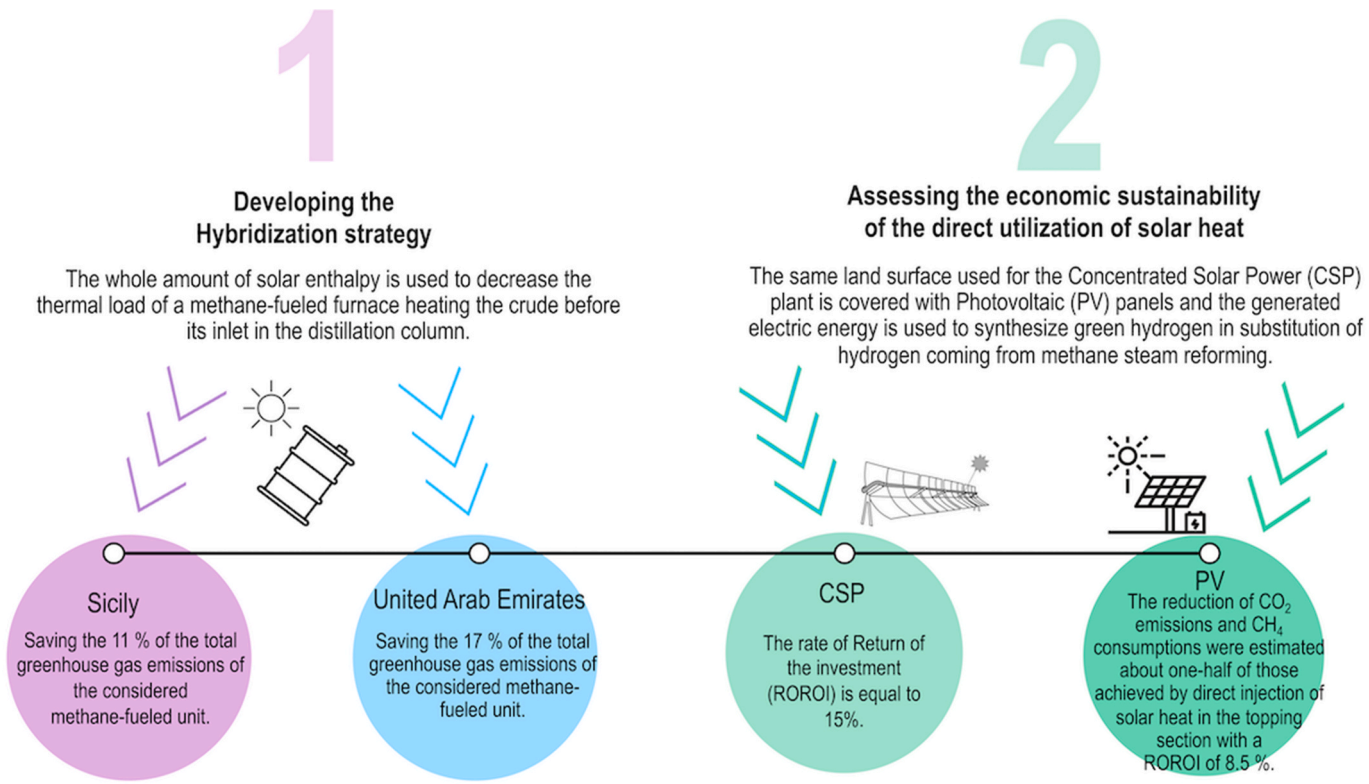

Fig. 11. Graphical summary of the main results of the study.

CRediT authorship contribution statement

Claudia Prestigiacomo: Writing – original draft, Software, Methodology, Investigation, Conceptualization. **Alberto Giaconia:** Writing – original draft, Investigation, Conceptualization. **Federica Proietto:** Methodology, Investigation. **Giampaolo Caputo:** Software, Methodology, Investigation. **Irena Balog:** Investigation. **Egnazio Ollà:** Writing – original draft, Methodology. **Chiara Freni Terranova:** Investigation. **Onofrio Scialdone:** Validation, Investigation, Formal analysis. **Alessandro Galia:** Writing – review & editing, Validation, Supervision, Funding acquisition, Conceptualization.

Declaration of competing interest

The authors declare the following financial interests/personal relationships which may be considered as potential competing interests: Alessandro Galia reports financial support was provided by European Commission. Alessandro Galia reports financial support was provided by Government of Italy Ministry of Economic Development.

Data availability

Data will be made available on request.

Acknowledgements

The results presented in this paper have been obtained in the framework of the "Concentrating Solar Power" project, under the "Electric System Research" program 2019–2021, with the financial support of Italian Ministry for Ecological Transition and in the framework of Project code PE0000021, Concession Decree No. 1561 of 11.10.2022 adopted by *Ministero dell'Università e della Ricerca* (MUR), CUP B73C22001280006, Project title "Network 4 Energy Sustainable Transition – NEST".

Appendix A. Supplementary data

Supplementary data to this article can be found online at https://doi.org/10.1016/j.energy.2024.130718.

References

[1] World energy Outlook 2023. IEA Publications, International Energy Agency; 2023.
[2] Vooradi R, Anne SB, Tula AK, Eden MR, Gani R. Energy and CO_2 management for chemical and related industries: issues, opportunities and challenges. BMC Chemical Engineering 2019:1.
[3] IEA. The future of petrochemicals: towards more sustainable plastics and fertilisers. 2018. https://doi.org/10.1787/9789264307414-en.
[4] Energy Information Administration U. S. Annual energy Outlook 2023. Narrative; 2023. https://www.eia.gov/outlooks/aeo/.
[5] Zinoviev S, Müller-Langer F, Das P, Bertero N, Fornasiero P, Kaltschmitt M, Centi G, Miertus S. Next-generation biofuels: survey of emerging technologies and sustainability issues. ChemSusChem 2010;3:1106–33.
[6] Kumar N, Sonthalia A, Pali HS. Sidharth. Next-generation biofuels—opportunities and challenges. In: Green energy and technology. Springer Verlag; 2020. p. 171–91.
[7] Wang J, O'Donnell J, Brandt AR. Potential solar energy use in the global petroleum sector. Energy 2017;118:884–92.
[8] Altayib K, Dincer I. Analysis and assessment of using an integrated solar energy based system in crude oil refinery. Applied Thermal Engineering 2019;159:113799.
[9] Khan NA, Hussain Khoja A, Ahmed N, Riaz F, Mahmood M, Ali M, Kalam MA, Mujtaba MA. Solar-assisted hybrid oil heating system for heavy refinery products storage. Case Studies in Thermal Engineering 2023;49:103276.
[10] Mokhtari Shahdost B, Jokar MA, Razi Astaraei F, Ahmadi MH. Modeling and economic analysis of a parabolic trough solar collector used to preheat the process fluid of furnaces in a refinery Case study: Persian Gas Refinery. Journal of Thermal Analysis and Calorimetry 2019;137:2081–97.
[11] Ahmadi H, Behbahani-Nia A, Torabi F. Technoeconomic analysis of combined heat and power generation systems with regard to solar energy for lubricant oil refinery utilization. Energy Sources, Part B: Economics, Planning, and Policy 2017;12:605–13.
[12] U.S. Department of Energy (DOE). Energy and environmental profile of the U.S. petroleum refining industry. https://www.energy.gov/eere/amo/petroleum-refining; 2007.
[13] Mathew TJ, Narayanan S, Jalan A, Matthews L, Gupta H, Billimoria R, Pereira CS, C G, Tawarmalani M, Agrawal R. Advances in distillation: significant reductions in energy consumption and carbon dioxide emissions for crude oil separation. Joule 2022;6:2500–12.
[14] Abikoye B, Cucek L, Isafiade AJ, Kravanja Z. Integrated design for direct and indirect solar thermal utilization in low temperature industrial operations. Energy 2019;182:381–96.
[15] Ismail MI, Yunus N Al, Hashim H. Integration of solar heating systems for low-temperature heat demand in food processing industry – a review. Renewable and Sustainable Energy Reviews 2021;147:111192.
[16] Tasmin N, Farjana SH, Hossain Md R, Golder S, Mahmud MAP. Integration of solar process heat in industries: a review. Clean Technol 2022;4:97–131.
[17] Goel A, Manik G, Verma OP. Integration of a parabolic trough solar collector with an energy-intensive multi-effect evaporator: a move towards industrial decarbonization. Energy 2023;279:128058.
[18] Giaconia A, Iaquaniello G, Metwally AA, Caputo G, Balog I. Experimental demonstration and analysis of a CSP plant with molten salt heat transfer fluid in parabolic troughs. Solar Energy 2020;211:622–32.
[19] Giaconia A, Tizzoni AC, Sau S, Corsaro N, Mansi E, Spadoni A, Delise T. Assessment and perspectives of heat transfer fluids for csp applications. Energies 2021;14:7486.
[20] Dribssa E, Cogliani E, Lavagno E, Petrarca S. A modification of the heliostat method to improve its performance. Solar Energy 1999;65:369–77.
[21] Giaconia A, Caputo G, Ienna A, Mazzei D, Schiavo B, Scialdone O O, Galia A. Biorefinery process for hydrothermal liquefaction of microalgae powered by a concentrating solar plant: a conceptual study. Applied Energy 2017;208:1139–49.
[22] Aspen Plus ®, "Getting started modeling Petroleum processes" report [18]. Version V7.1.
[23] Miliozzi A, Giannuzzi GM, Tarquini P, La Barbera A. ENEA Progetto solare ad alta temperatura: Fluido termovettore: dati di base della miscela di nitrati di sodio e potassio. ENEA/SOL/RD/2001/07; 2001. Rev. 0.0.
[24] Darío Gómez AR, Watterson Branca B, Americano JD, Ha C, Marland G, Matsika E, Nenge Namayanga L, Osman-Elasha B, Kalenga Saka JD, Treanton K. Chapter 2: Stationary Combustion 2006 IPCC guidelines for National greenhouse gas Inventories. Energy 2.2 2 2006. https://www.ipcc-nggip.iges.or.jp/public/2006gl/pdf/2_Volume2/V2_2_Ch2_Stationary_Combustion.pdf.
[25] International Renewable Energy Agency. The power to change: solar and Wind cost reduction potential to 2025. 2016. https://www.irena.org/-/media/Files/IRENA/Agency/Publication/2016/IRENA_Power_to_Change_2016.pdf.
[26] Sun P, Young B, Elgowainy A, Lu Z, Wang M, Morelli B, Hawkins T. Criteria Air Pollutants and greenhouse gas emissions from hydrogen production in U.S. Steam methane reforming Facilities. Environmental Science Technology 2019;53:7103–13.
[27] Wanner M. Transformation of electrical energy into hydrogen and its storage. The European Physical Journal Plus 2021;136.
[28] Van de Voorde M. Hydrogen production and energy Transition. De Gruyter; 2021.
[29] International Renewable Energy Agency. Green hydrogen cost reduction scaling up electrolyzers to meet the 1.5°C climate goal. 2020. https://www.irena.org/-/media/Files/IRENA/Agency/Publication/2020/Dec/IRENA_Green_hydrogen_cost_2020.pdf.
[30] Vartiainen E, Masson G, Breyer C, Moser D, Román Medina E. Impact of weighted average cost of capital, capital expenditure, and other parameters on future utility-scale PV levelised cost of electricity. Progress in Photovoltaics: Research and Applications 2020;28:439–53.
[31] Curtis T, Heath G, Walker A, Desai J, Settle E, Barbosa C. Best Practices at the end of the photovoltaic system performance period. 2021. NREL/TP-5C00-78678, https://www.nrel.gov/docs/fy21osti/78678.pdf.